We are IntechOpen,
the world's leading publisher of
Open Access books
Built by scientists, for scientists

6,900
Open access books available

186,000
International authors and editors

200M
Downloads

154
Countries delivered to

Our authors are among the

TOP 1%
most cited scientists

12.2%
Contributors from top 500 universities

CLARIVATE ANALYTICS
BOOK CITATION INDEX
INDEXED

WEB OF SCIENCE™

Selection of our books indexed in the Book Citation Index
in Web of Science™ Core Collection (BKCI)

Interested in publishing with us?
Contact book.department@intechopen.com

Numbers displayed above are based on latest data collected.
For more information visit www.intechopen.com

Nondestructive Characterization of Drying Processes of Colloidal Droplets and Latex Coats Using Optical Coherence Tomography

Yongyang Huang, Hao Huang, Zhiyu Jiang, Lanfang Li, Willie Lau, Mohamed El-Aasser, Hsin-Chiao Daniel Ou-Yang and Chao Zhou

Abstract

In this chapter, we review the applications of optical coherence tomography (OCT) on the nondestructive characterization of the drying processes of colloidal droplets and latex coatings. Employing time-lapse, high-speed imaging, OCT can be used to monitor the dynamic process of drying colloidal droplets. With the aid of high-scattering, micron-sized tracer particles, fluid flows have been captured; phase boundaries are also visible in liquid crystal droplets; and the speckle contrast analysis differentiates the dynamics of particles, showing the packing process and the coffee ring phenomenon. In a waterborne latex coat, time-lapse OCT imaging reveals spatial changes of microstructures, i.e., detachment of latex, cracks, and shear bands; with speckle contrast analysis, 1D and 2D particles' packing process that is initiated from latex/air interface can also be monitored over time. OCT can serve as an experimental platform for fundamental studies of drying colloidal systems. In the future, OCT can also be employed as an in-line quality control tool of polymer coatings and paints for industrial applications.

Keywords: optical coherence tomography, drying, colloidal droplet, waterborne latex, liquid crystal droplet, time-lapse imaging, speckle

1. Introduction

In this chapter, we describe the applications of optical coherence tomography (OCT) on the characterization of drying dynamics of colloidal systems. Specifically, we will use OCT in combination with other modalities (i.e., gravimetry and video recording) to characterize two drying models: (1) drying colloidal droplets and (2) drying latex coat. The entire drying processes of these systems can take from a few minutes for microliter droplets to a few hours or days for thick-film latex in Petri dishes. Given the high-speed imaging capability with a temporal resolution on the order of milliseconds, OCT can detect the flow of fluid or particle motions. Given the nondestructive nature of OCT, time-lapse OCT can be used to monitor the drying processes of droplets and latex coats.

2. Drying process of colloidal droplets

Drying of the colloidal droplets has been a subject of great interest since the 1980s [1]. Studies of a drying droplet, including changes of drying rate and contact angle, the progression of its shape, and final deposition pattern, can help us understand many interesting phenomena, such as coffee ring effects [2], electro-wetting effects [3], and Marangoni effects that are driven by surface tension gradients [4]. Mechanisms behind these phenomena may involve a complex interplay of convection and evaporation, surface tension and capillary force, particles' interactions, rheology, substrate hydrophobicity, pinning of the contact line, and Marangoni forces [3, 5]. During drying, unlike pure water droplets, the constituents in colloidal droplets, including various concentrations of particles [6], polymers [7–9], surfactants [10], solvents [11], and salts [12] will alter the interactions among these mass transfer mechanisms, yielding different drying behaviors. Additionally, environmental conditions such as temperature and humidity and the substrate properties also affect the drying process and final deposition [13, 14]. Insights gained from these studies of evaporating droplets may ultimately translate to practical applications in polymer science, biomedicine, and nanotechnology [14], such as inkjet printing [15], DNA chip [16], biosensor [17, 18] and disease diagnosis based on deposition pattern of biological fluid [19–22], food quality analysis [23], particle separation [24], and production of nanoparticles for drug delivery [25, 26]. All above-mentioned applications are related to mass transportation during drying of a liquid suspension and the resultant film property.

Using OCT to monitor the drying process of colloidal droplets has been conducted in a few studies. **Table 1** summarizes the details of experimental designs for these studies. In conjunction, **Figure 1** illustrates the schematics of the drying process of these colloidal droplet models.

Trantum et al. demonstrated the first study to utilize OCT to visualize the cross-section of drying water droplets with suspended particles (see **Figure 1A**) [27]. Low concentration of polystyrene, melamine formaldehyde, or silica particles with a diameter of 1 μm and a volume fraction of 0.005% was suspended in distilled water. The water droplet was loaded on a hydrophilic glass slide. The drying experiment was conducted in the ambient condition with relative humidity (RH) controlled to 30 or 40%. A commercial spectral-domain OCT system with a central wavelength of 860 nm and a spectral bandwidth of 51 nm was used to image the droplet. Axial and lateral resolutions of the OCT system were 6.4 and 8 μm, respectively. The scan rate of the system was set to 10 kHz. Their results showed that both the sedimentation rate and evaporation rate would affect the drying dynamics of particle-containing water droplets. In fast evaporating mode, the descending rate of drop surface was faster than the rate of particle sedimentation, resulting in the particles being trapped at the air-water interface (top surface). Close to the water-substrate interface, the "coffee ring" flows (CF) played a major role to transport the particles to the pinned contact line, yielding a "coffee ring" final deposition pattern. Given the same particle size, increased particle densities, i.e., silica (2.00 g/cm^3), as compared to polystyrene (1.04 g/cm^3) lead to early sediment of particles and early transportation of particles to the edge by "coffee ring" flows. Their results suggested a way to control the final deposition of coffee ring structure based on particles' density.

Based on the previous observations of drying colloidal droplets, the same group proposed design of biosensor utilizing the final deposition pattern to track the existence and concentration of target biomarkers (**Figure 1B**) [17]. In the experiment, the tracer particles were coated with antibodies. These particles would aggregate in the presence of target biomarker (M13 bacteriophage in the study). Polydimethylsiloxane (PDMS) with low thermal conductivity (0.15 W/mK) was

References	Trantum et al. [27]	Trantum et al. [17]	Manukyan et al. [28]	Davidson et al. [3]	Edwards et al. [29]	Huang et al. [30]
Years	2013	2014	2013	2017	2018	2018
Suspended materials	PS, MF, Si*	Monoclonal antibodies Glycerol with M13**	Model paint	LCLC, SSF***	Binary drops (ethanol and n-butanol)	PS Latex
Diameter (nm)	1000	1000	<1000	N.A.	N.A.	L Latex 125 S Latex 53
Initial concentration	vol%: 0.005% (10^5/μL)	vol%: 0.05% (10^6/μl) Glycerol: 8%	vol%: 10, 30, 50%	wt%: 5–20%	wt%: 2–20%	wt%: L latex: 40.11%, S latex: 33.43%
Substrate	Glass slide	PDMS	Glass coated by Tegotop® 210	Glass slide and coverslip	Glass coated by Flutech LE15	Glass slide
Environment	Ambient	Ambient	Ambient	Chambered	Chambered	Ambient
Droplet model	Sessile	Sessile	Sessile	Sessile	Sessile or pendant	Sessile
Transparency****	Transparent	Transparent	Opaque	Transparent	Transparent	Opaque
Tracers	None		Copolymer microspheres diameter: 4.3 or 7.9 μm	Polystyrene diameter: 1 μm	0.01 wt% polystyrene diameter: 2 μm	None
OCT type	Spectral domain		Spectral domain	Spectral domain	N.A.	Spectral domain
λ_{OCT} (nm)	860		930	800	1300	1320
$\Delta\lambda_{OCT}$ (nm)	51		100	220	N.A.	110
Axial and lateral resolutions (in air)	6.4 μm 8 μm		7 μm 9 μm	1.9 μm 3.5 μm	5.5 μm 13 μm	6.8 μm 14 μm
Scan speed (kHz)	10		N.A.	20	N.A.	20.7
Imaging depth and scan range	N.A.		1.6 mm 4 mm	N.A.	N.A. 2.5 mm	2.2 mm 5.0 mm

References	Trantum et al. [27]	Trantum et al. [17]	Manukyan et al. [28]	Davidson et al. [3]	Edwards et al. [29]	Huang et al. [30]
Frame rate or time interval	5 or 0.5 fps, 200 frames		2 fps	33 or 50 fps interval: ~3–4 s	50 fps	Interval: ~10 s

*PS: polystyrene, MF: melamine formaldehyde, Si: silica.
**Particle surface was functionalized with anti-M13.
***LCLC: lyotropic chromonic liquid crystal. SSF: sunset yellow FCF.
****Optical transparency in near-IR wavelength range.

Table 1.
OCT studies on drying droplets.
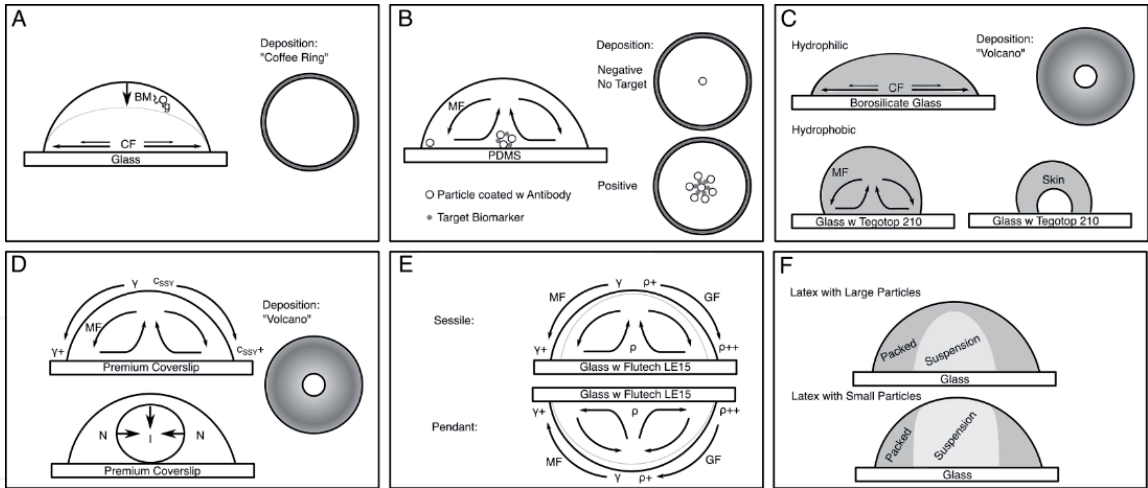
Figure 1.
Illustrations of drying process of six colloidal droplet models. (A) Water droplets with tracer particles, i.e., polystyrene, melamine formaldehyde, silica. (B) Water droplet with antibody-coated particles to detect biomarkers. (C) Model paint droplet. (D) Liquid crystal droplet. (E) Binary liquid droplet. (F) Waterborne latex droplet.

used as the substrate. Thus, a temperature gradient was established along with the interface, inducing a surface tension gradient and promoting Marangoni flows. During the drying process, the particle aggregates in the presence of biomarkers showed a thicker convective flow pattern in the cross-sectional OCT images, while the dispersed particles showed a uniformly distributed convective flow pattern in the absence of biomarkers [17]. Under the influence of Marangoni flows, increase of viscosity by glycerol, and effect of gravity, the particle aggregates were concentrated and deposited at the droplet center, forming a concentric final deposition pattern. Note that, with the glass substrate, the particle aggregates will not concentrate at the droplet center.

Manukyan et al. reported using OCT to characterize the internal flows in a drying model paint droplet (**Figure 1C**) [28]. Commercial model paint droplets with various initial volume fractions were characterized. Copolymer microspheres were mixed in the model paint droplets as tracer particles. Model paint droplets with an initial volume of 5–8 μL were loaded on hydrophilic or hydrophobic substrates, and their drying behaviors were monitored separately. A spectral-domain OCT system was utilized to perform time-lapse imaging of model paint droplets. The central wavelength and the spectral bandwidth of the system were 930 and 100 nm. Axial and lateral resolutions of the OCT system were 7 and 9 μm, respectively. The OCT system can scan a maximum transverse range of 4 mm. In their results, the model paint droplets on a hydrophilic substrate exhibited an outward radial flow pattern and a donut-shaped final deposition pattern in cross-sectional OCT images, indicating that the drying processes of these droplets were driven mainly by the coffee ring effect. However, on the hydrophobic surface, a reversed Marangoni flow was established in the drying of model paint droplets, shown as the convective flow moving down along the surface and then moving inward along the droplet-substrate interface in the OCT image. As the model paint droplet continued to dry, the formation of a skin layer was observed inside the droplet. At this stage, no convective flows were observed. A cavity was observed beneath the outer skin layer in OCT cross-sectional images.

Davidson et al. investigated the drying process of water droplets containing lyotropic chromonic liquid crystals (LCLCs), using polarized optical microscopy (POM) and OCT (**Figure 1D**) [3]. LCLCs are composed of organic, charged, and plank-like molecules [31, 32]. During the drying process of LCLC containing

droplets, changes of local temperature and concentration of LCLCs induce multiple phases of the LCLCs, including isotropic, nematic, columnar, and crystalline phases [3]. In the experiment, a droplet containing sunset yellow FCF (SSY), a dye that belonged to LCLC family, was loaded on a premium coverslip of the substrate. Polystyrene particles were added in the droplets as tracers to track fluid flows. A semi-enclosed PDMS chamber was used to slow down the drying rate, yielding a total drying time of ~10–15 min for the LCLC containing droplets with an initial volume of ~0.2–0.5 µL. To visualize the small tracer particles in the LCLC containing droplet, an ultrahigh-resolution (UHR) spectral-domain OCT system was employed, with a central wavelength of 800 nm and a spectral bandwidth of 220 nm. Axial and lateral resolutions of the UHR-OCT system were 1.9 µm and 3.5 µm, respectively. The camera's scan rate was set to 20 kHz. **Figure 2** shows the development of drying SSY solution droplet by UHR-OCT. High-speed time-lapse OCT imaging showed that the convective flows were initiated right after the SSY solution droplet was loaded on the substrate. Substantial Marangoni flows were visualized in time-lapse OCT images, which were established due to the increased concentration of SSY particles near the pinned contact line during the evaporation, leading to increase in local surface tension gradient along with the droplet interface. In the next stage, the formation of the nematic phase (N) pushed the isotropic (I)-nematic phase boundary to the center. Finally, the isotropic phase diminished at the droplet center. A volcano-shaped final deposition pattern is observed for SSY solution droplets.

Recently, Edwards et al. utilized OCT to investigate the flow patterns of the drying binary liquid droplets (**Figure 1E**) [29]. Low concentration of solvents, i.e., ethanol or n-butanol, was diluted in the water solution to form binary liquid droplets. To monitor the drying binary liquid droplets, a 1300 nm OCT system was employed, with an axial resolution of 5.5 µm and a lateral resolution of 13 µm.
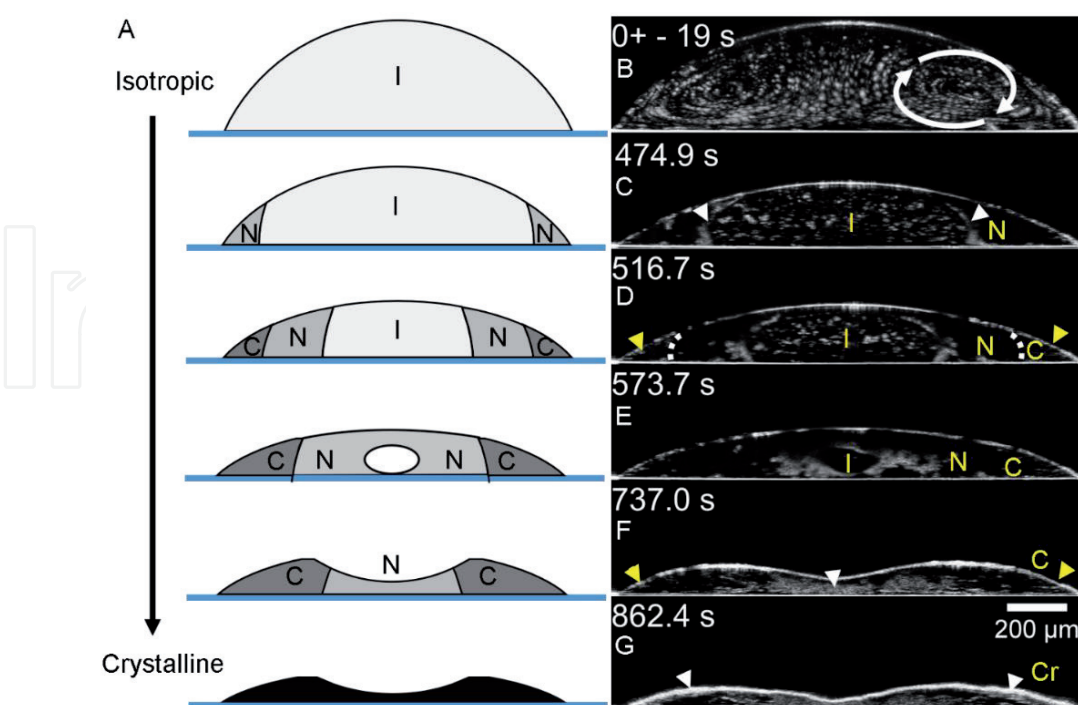
Figure 2.
Drying process of SSY solution droplet imaged by ultrahigh-resolution optical coherence microscopy (UHR-OCM). A schematic illustration of phase behaviors of SSY solution droplet at different drying stages was shown in (A). (B–G) UHR-OCM images of the SSY solution droplet at different drying time points. White spots: polystyrene particles as tracers. Cr: crystalline. C: columnar. N: nematic. I: isotropic. White dashed line in (D): columnar-nematic boundary. White arrows in (C): nematic-isotropic boundary. Yellow arrows: columnar line structures. White arrow in (G). Crystallized state. Image reproduced from Ref. [3].

A scan range of 2.5 mm was set, which was sufficient to cover the whole droplet. Different from the previous three studies, they investigated the flow pattern under different tilting conditions, including the sessile droplet mode with 0° tilting and pendant droplet mode with 180° tilting. In the tilted configuration, axisymmetric toroidal flow patterns were observed by OCT in the middle of drying processes. In the sessile droplet, a convective flow pattern in the same direction as expected by Marangoni driven flow was observed. However, in the pendant droplet, the flow direction was opposite to the Marangoni flow direction, suggesting that Marangoni flows might not dominate in the evaporating binary liquid droplets. They suggested that the convective flows were driven by the density of the liquid and gravity. In the case of the water-ethanol droplet with the preferential evaporation of ethanol, the binary liquid close to the air-water interface was denser than the bulk. Thus, surficial binary liquids would fall along the air-water interface from top to edge in sessile droplets and from edge to bottom in the pendant droplets, driving convective flows in different patterns. Also, they monitored the full drying process of the binary liquid droplets with OCT, showing a three-stage drying process, which are chaotic flows, convective flows, and outward "coffee ring" flows.

3. Drying process of colloidal latex droplets

A latex (or emulsion polymer) is a stable colloidal system with polymer particles suspending in an aqueous solution. The size of polymer particles ranges from a few nanometers to a few hundred, and the sedimentation can be neglected [31, 33]. A latex is usually synthesized by the emulsion polymerization procedure [31, 34]. Thanks to their ability of film formation, latexes can be used in application including the binder in waterborne paints [35], waterborne pressure-sensitive adhesives [36], inkjet printing [37, 38], sunscreen [39], paper coating [40, 41], drug tablet coating [42, 43], carpet backing [44], and evaporative lithography [45–47].

Drying process of latex is inhomogeneous. That is, latex particles distribute nonuniformly, spatially, and temporally. As the latex continues drying, the inhomogeneous distribution can lead to the formation of drying defects. The drying inhomogeneity can occur in both horizontal and vertical directions. In the horizontal direction, the evaporation rate is faster on the droplet edge than in the center. Further, the "coffee ring" flows drive the particles from the center to the edge, resulting in a final "coffee ring" deposition pattern, an uneven coating surface [32, 48, 49]. In the vertical direction, particles aggregate on the top surface, forming a "skin layer" that inhibits the drying process [33, 50–54]. Furthermore, if the glass-transition temperature (T_g) of particles is above room temperature, particles are stiff, and cracks would be seen in the latex [54–58]. To create uniform evaporation, it is important to understand and characterize the drying latex with different T_g, particle size and surfactant concentrations.

Using OCT to characterize the drying process of the waterborne latex droplets has been an active research effort, with an emphasis on observing drying inhomogeneity. In recent studies by Huang et al. [54, 59], the waterborne latex droplets contained polystyrene particles with different sizes, initial solid contents, and surfactant solid contents (L latex: particle size, ~125 nm; initial solid content, 40.11 wt%; surfactant solid content, 0.2 wt%. S latex: particle size, ~53 nm; initial solid content, 33.43 wt%; surfactant solid content, 1.4 wt%). To monitor the drying process of the latex droplets, the integrated OCT-gravimetry-video platform [30] was employed. The spectral-domain OCT system in the integrated platform had a central wavelength of 1320 nm and a spectral bandwidth of 110 nm. Axial and

lateral resolutions of the system were 6.8 μm and 14 μm, respectively. The camera's scan rate was set to 20.7 kHz. The maximum imaging depth and lateral scan range were 2.2 mm and 5 mm. In the experiments, latex droplets with a volume of ~5 μL were loaded on a cleaned glass slide. Experiments were conducted in the ambient condition. The total drying time for both L and S latex droplets were ~13–15 min. Time-lapse, M-mode (repeated frames) OCT imaging was initiated after ~80 s from the loading of latex droplets, with a time interval of ~10 s.

Figure 3 showed time-lapse OCT imaging of drying L and S latex droplets. In **Figure 3A** and **B**, a domain boundary was clearly observed inside the L latex droplet with distinct scattering properties. The outer layer had lower scattering intensity, and inner layer had higher scattering intensity. OCT speckle contrast analysis [30, 54] was further carried out on the same data. In the outer layer, the higher speckle contrast indicated that motions of particles in these regions were restricted. The dark center inside the L latex droplet inferred that the particles were active in Brownian motions. With these analyses, we confirmed our observation that particles' packing occurred from the droplet edges and propagated inward, similar to the drying latex coat in the Petri dish [30]. The packing of particles was also observed in S latex droplet, in both OCT structural images (**Figure 3D–F**) and speckle images (**Figure 3J** and **K**). Particles began packing on the air/latex interface. In **Figure 3I**, we observed that the horizontal packing process was much faster than the vertical packing process in L latex, which was attributed to faster evaporation rate at the pinned contact line at droplet edge than the apex of the droplet. In S latex droplet, the vertical packing process was delayed as compared to the horizontal packing process. At ~410 s, we could barely see a thin layer in **Figure 3F**, indicating the existence of a vertical packed layer. The vertical layer was clearly visible until ~500 s. As a comparison, the vertical packed layer was clearly visible in the L latex droplet at ~300 s. This can be explained by the difference of diffusivity ($D = k_B T/6\pi\eta R$) [60]. Larger particles have less diffusivity than small particles, and thus small particles tend to counteract the drying and impede the packing process on the top. The particle droplets were fully packed at ~410 s for L latex droplet and ~630 s for S latex droplet.
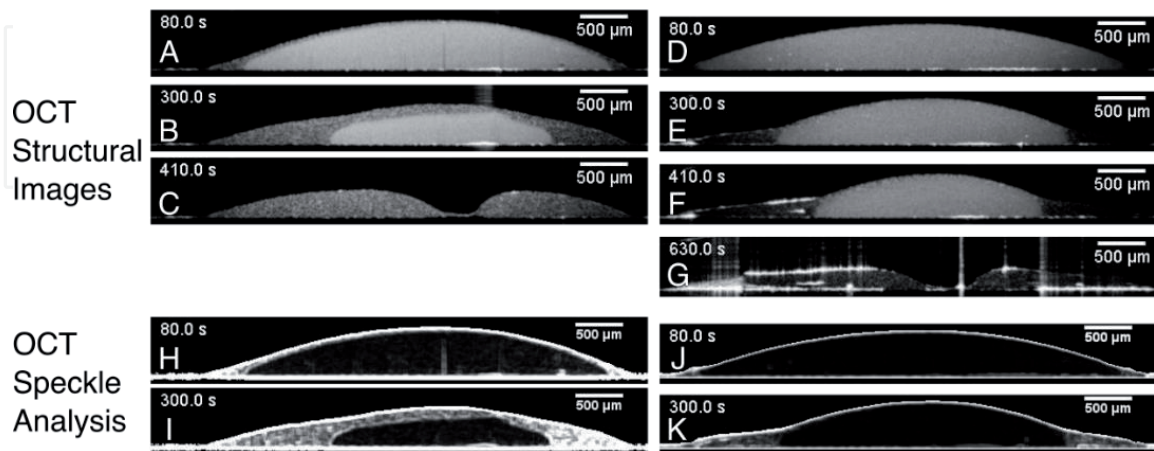
Figure 3.
Drying progression of latex droplets showing the horizontal and vertical packing process. ~5 μL latex droplets containing larger (L latex; particle diameter, ~125 nm) and smaller (S latex; particle diameter, ~53 nm) polystyrene particles were loaded on the glass slide, with initial solid contents of 40.11 and 33.43 wt%, respectively. OCT structural images of L (A–C) and S (D–G) latex droplets clearly showed domain boundaries between surficial packed region close to air-latex interface and inner suspension regions with different scattering properties. OCT speckle contrast analysis (H–K) further confirmed the inhomogeneous particles' packing process for L and S latex droplets, with different particles' mobilities in the packed and suspension regions. Image cited from Refs. [54, 59].

To sum up, the utilization of OCT was demonstrated to reveal the drying inhomogeneity in waterborne polystyrene latex droplets. The time-lapse OCT results showed that both L and S latex droplets exhibit particles packing processes in horizontal and vertical directions, but with a difference of packing speed between them. This high T_g particle can be seen as a model system to illustrate the effect of particle compaction only without the complication of particle consolidation or deformation. Further research using low T_g latex particles can potentially shine light on the full process of film formation, including particle compaction and consolidation.

4. Drying process of latex coats

OCT can also be employed to monitor the drying process of the latex coat. As shown in **Figure 4A**, OCT scans a small area on a large uniform latex coat in a Petri dish. Given the nondestructive-imaging capability, OCT can perform the cross-sectional imaging of the drying process of latex coat that simulates the real paint/coating applications and provide a characterization of internal structures, different drying behaviors, and drying inhomogeneity along the vertical direction of the latex coat. Previously, Lawman and Liang [61] and Saccon et al. [62] have reported using OCT to monitor the drying process of varnish, in which average refractive index, surface roughness, and thickness have been characterized. Huang et al. furthers the application of OCT on investigating the drying phenomena of latex coat, including the cross-sectional imaging and particles' dynamics analysis [30, 54].

Combining OCT with gravimetric and video measurements can fully characterize the drying process of polystyrene latex coat [30]. Among these modalities, time-lapse OCT imaging can show the local microstructures, 1D vertical drying process, and drying inhomogeneity from the cross-sectional view of the drying latex. **Figure 4** shows a representative OCT imaging of a latex coat containing polystyrene particles (L latex). The composition of L latex coat with particle size ~125 nm is the same as the colloidal latex droplet in Section 3. The L latex coat was loaded in an 8.5-cm-diameter Petri dish, with an initial thickness of ~1 mm. The visual appearance of a drying latex coat is presented in **Figure 4A**, with solid content (k_s) of 42.9 wt% at ~30 min. **Figure 4B** shows time-lapse OCT characterization result of the full drying process of the L latex coat. On the top of the time-lapse OCT intensity profile, four drying stages were labeled based on OCT observations of drying phenomena, including the packing process, consolidation, stress relaxation, and final drying stage. In **Figure 4B**, a linear decrease of the thickness of the L latex coat in the packing stage and the detachment of the latex film bottom in the stress relaxation stage were shown. During the stress relaxation stage, the scattering intensities change, suggesting the rearrangement of particles to release the internal stress accompanied by the infiltration of air. In the final drying stage, the latex coat remains uniform without any significant changes of the scattering intensity or thickness.

Figure 4C shows a demonstration of OCT to visualize particles' packing process in L latex coat. In zoomed-in time-lapse OCT intensity profile within the first ~180 min (**Figure 4C**, top), the separation of packed and suspension layers can be seen based on the scattering light intensity variation. The packed/suspension domain boundary is visible and highlighted by a dotted curve. Next, a speckle contrast analysis [30] identifies particles' dynamics in these two domains. In time-lapse OCT speckle image (**Figure 4C**, bottom), the particles' dynamics in these two domains can be clearly distinguished. In the upper domain, the high speckle contrast (K_s) indicates that particle
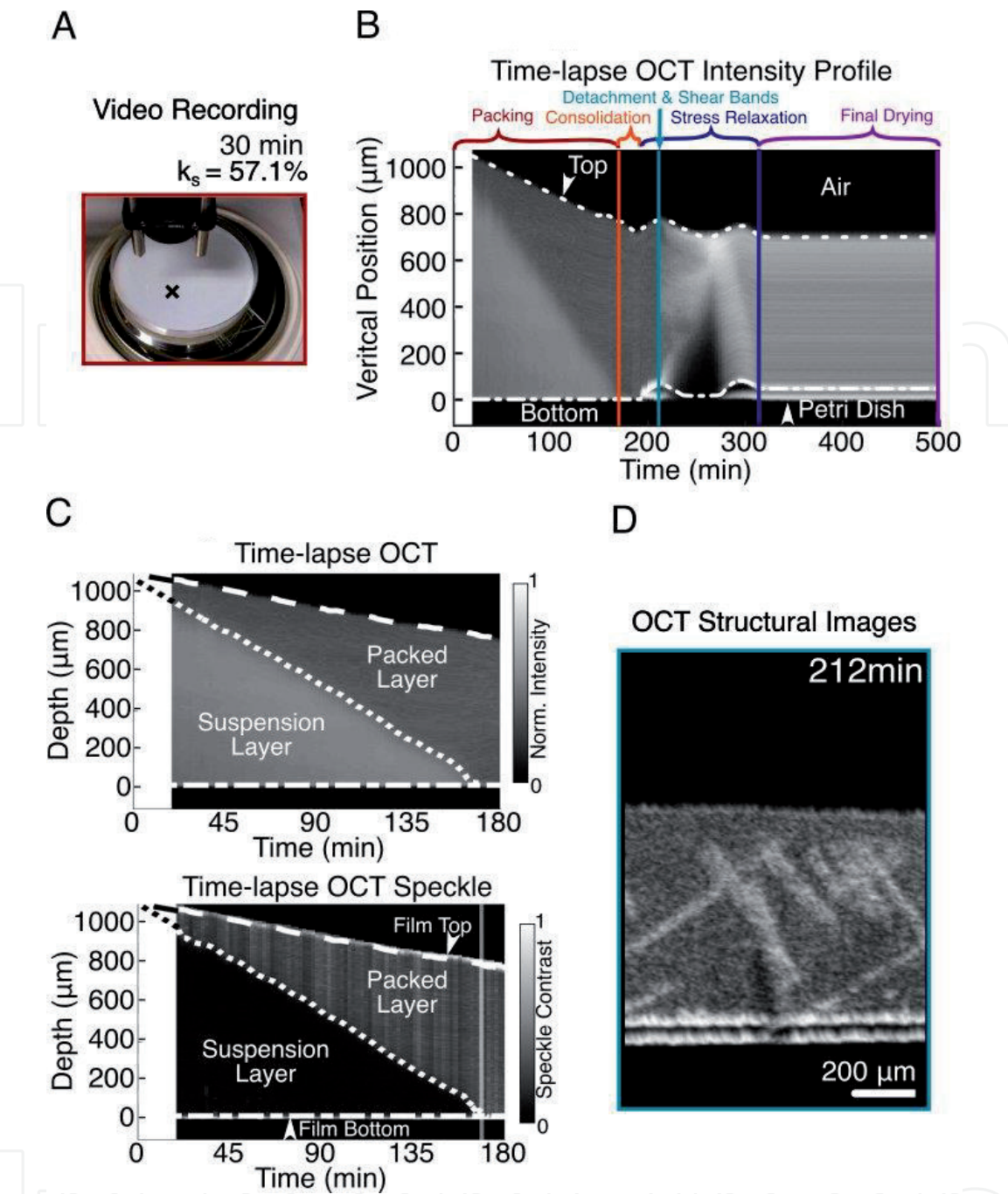
Figure 4.
OCT characterization of drying process of a polystyrene latex in Petri dish. (A) Visual appearance of the drying latex coat at ~30 min. (B) Time-lapse OCT intensity profile showing the drying process of the latex coat. (C) Visualization of particles' packing process of latex coat in time-lapse OCT intensity profile (top) and in time-lapse OCT speckle profile (bottom). (D) Visualization of latex detachment and formation of shear-band structures in 2D OCT structural image. Image reproduced from Ref. [30].

movement is restricted in the packed layer. Conversely, the low K_s value in the lower domain infers that these particles are freely moving in the suspension layer. Based on speckle contrast, the packed/suspension domain boundary can be easily identified and plotted. After the domain boundary is identified, the packed layer thickness changes can be derived from the time-lapse OCT speckle image.

Formation of shear bands is observed in the polystyrene latex coat, shown in 2D OCT structural image in **Figure 4D**. At ~212 min, the shear-band structure starts to form, indicated by the bright crosses inside the latex. The observed shear-band structure in cross-sectional OCT image is similar to the shear-band structure investigated by Yang et al. [63] and Kiatkirakajorn and Goehring [64]. The shear band is postulated to be attributed to the dislocation of packed latex particles due to the internal

compressive stress along the vertical direction. These dislocations allow the air to infiltrate, resulting in a high refractive index mismatch between the air and the latex polymer or water in the dislocation, making the shear bands visible under OCT [30].

5. Discussions

In the previous sections, the feasibility of OCT is shown to characterize the drying processes of colloidal droplets and latex coats. OCT can provide cross-sectional views to observe the internal structures of the colloidal droplets and latex coats. Novel observations of shear-band structure and particles' packing process in the latex coat are shown. Based on the cross-sectional images, quantitative analyses can be conducted on drying droplets and latex coats, including contact angle of the droplet and the thickness of the latex coat. With the high-speed imaging capability, OCT can track different types of fluid flows with the aid of micron-sized tracer particles, especially the convective fluid flow. By doing the speckle contrast analysis, the packing process and the coffee ring phenomenon can be accurately imaged. The nondestructive nature of OCT enables monitoring of a full drying process to reveal the time-dependent changes, such as the phase changes of liquid crystal droplets and the consolidations of latex particles. Taken all these advantages, OCT can play an important role in fundamental studies of drying colloidal droplets and latex coats.

In OCT images of the drying colloidal materials, the fluid flows have been visualized by tracking the trajectories of micron-sized tracers. The choice of the tracers in colloidal droplets depends on the optical transparency as well as the OCT system resolutions in both axial and lateral resolutions. Empirically, the colloids with a low initial concentration of suspended materials are transparent, and the colloids with a high concentration of suspended materials (e.g., colloidal latex droplets) are semitransparent or opaque. In order to distinguish the tracers, the light scattering properties (e.g., refractive index) of the tracers should be significantly different from the bulk colloidal droplet. Based on light scattering properties, polystyrene, gold, and titanium oxide (TiO_2) particles can be potential candidates for tracers. The size of tracers should be close to the OCT system resolution to resolve individual tracers.

For latex coats, the field of view (FOV) for a standard OCT system (a few millimeter square) only covers a small area of the latex coat. Expanding FOV for OCT systems may enable the observation of time-dependent horizontal drying inhomogeneity, such as drying front propagation. One simple approach to expand FOV is to use an objective with a lower numerical aperture, with a trade-off of the lateral resolution. An alternative approach is to utilize parallel beams to image the latex at different spots. A parallel-imaging OCT system with a space-division multiplexing technique was demonstrated by Huang et al. previously to perform wide-field imaging with simultaneous eight-channel illumination, covering an area of 18.0×14.3 mm^2 [65].

We should note that OCT measures the optical path length instead of absolute distance in the vertical direction. To derive the latex thickness, the measured optical path length value is divided by the predetermined refractive index values, assuming the refractive index remains relatively constant in space and time. Temporal and spatial variations of the refractive index, which is not considered in our experiments, may result in quantification errors in time-lapse thickness measurements.

6. Conclusions and future perspectives

In this chapter, recent progresses have been summarized on utilizing OCT for investigation of drying processes of the colloidal droplets and latex coats.

In colloidal droplets, high-speed OCT imaging can show different types of flows with the help of micron-sized tracer particles, involving the radial coffee ring flows, Marangoni flows, and density-driven flows. In addition, phase evolutions of liquid crystal droplets can be observed in OCT cross-sectional images. For colloidal latex droplets and latex coats, 1D or 2D particles' packing process can be visualized with speckle contrast analysis to characterize particles' dynamics, without adding any tracer particles. Long-term structural changes of drying latex can be investigated continuously, such as crack formation, detachment, and shear-band structures in the polystyrene latex. In these studies, the advantages of OCT are shown to provide the cross-sectional views of the droplets and latex coats with good depth-resolvability, deep penetration, good temporal resolution, and the capability of long-term, nondestructive characterization.

OCT has opened new opportunities to facilitate the fundamental studies of the interface and colloidal science to characterize different drying models. Other than sessile or pendant droplets, OCT can characterize levitated droplets to monitor different types of flows or particle motions. 1D confined droplet [66] or 1D confined flows in microfluidic channels can be imaged by OCT to characterize particles' dynamics. For latex coats, it is possible to explore the effects of additives (such as surfactant and water-soluble polymers) on the drying process of latex coats with the established integrated OCT system. In the future, OCT can be used as a tool for in-line evaluation of polymer coatings and paints for industrial applications.

Acknowledgements

Conflict of interest

The authors declare no conflict of interest.

Author details

Yongyang Huang[1], Hao Huang[2,3,4], Zhiyu Jiang[2], Lanfang Li[2], Willie Lau[5],
Mohamed El-Aasser[3,6], Hsin-Chiao Daniel Ou-Yang[2] and Chao Zhou[1,7]*

1 Department of Electrical and Computer Engineering, Lehigh University,
Bethlehem, PA, USA

2 Department of Physics, Lehigh University, Bethlehem, PA, USA

3 Department of Chemical and Bimolecular Engineering, Lehigh University,
Bethlehem, PA, USA

4 Axalta Coating Systems, Philadelphia, PA, USA

5 Beijing Oriental Yuhong Waterproof Technology Co., Ltd, Beijing, China

6 Department of Materials Science and Engineering, Lehigh University,
Bethlehem, PA, USA

7 Department of Biomedical Engineering, Washington University in St. Louis,
St. Louis, MO, USA

*Address all correspondence to: chaozhou@wustl.edu

IntechOpen

References

[1] Tarafdar S, Tarasevich YY, Dutta Choudhury M, Dutta T, Zang D. Droplet drying patterns on solid substrates: From hydrophilic to superhydrophobic contact to levitating drops. Advances in Condensed Matter Physics. 2018;**2018**:24

[2] Eral HB, Augustine DM, Duits MHG, Mugele F. Suppressing the coffee stain effect: How to control colloidal self-assembly in evaporating drops using electrowetting. Soft Matter. 2011;**7**:4954-4958

[3] Davidson ZS, Huang Y, Gross A, Martinez A, Still T, Zhou C, et al. Deposition and drying dynamics of liquid crystal droplets. Nature Communications. 2017;**8**:15642

[4] Jeong J, Davidson ZS, Collings PJ, Lubensky TC, Yodh AG. Chiral symmetry breaking and surface faceting in chromonic liquid crystal droplets with giant elastic anisotropy. PNAS. 2014;**111**:1742-1747

[5] Sadek C, Schuck P, Fallourd Y, Pradeau N, Le Floch-Fouéré C, Jeantet R. Drying of a single droplet to investigate process–structure–function relationships: A review. Dairy Science and Technology. 2015;**95**(6):771-794

[6] Deegan RD. Pattern formation in drying drops. Physical Review E. 2000;**61**(1):475-485

[7] Shimokawa Y, Kajiya T, Sakai K, Doi M. Measurement of the skin layer in the drying process of a polymer solution. Physical Review E. 2011;**84**(5):051803

[8] Anyfantakis M, Geng Z, Morel M, Rudiuk S, Baigl D. Modulation of the coffee-ring effect in particle/surfactant mixtures: The importance of particle-Interface interactions. Langmuir. 2015;**31**(14):4113-4120

[9] Kajiya T, Kaneko D, Doi M. Dynamical visualization of "coffee stain phenomenon" in droplets of polymer solution via fluorescent microscopy. Langmuir. 2008;**24**(21):12369-12374

[10] Gokhale SJ, Plawsky JL, Wayner PC. Spreading, evaporation, and contact line dynamics of surfactant-laden microdrops. Langmuir. 2005;**21**(18):8188-8197

[11] Kim H, Boulogne F, Um E, Jacobi I, Button E, Stone HA. Controlled uniform coating from the interplay of Marangoni flows and surface-adsorbed macromolecules. Physical Review Letters. 2016;**116**(12):124501

[12] Kaya D, Belyi VA, Muthukumar M. Pattern formation in drying droplets of polyelectrolyte and salt. Journal of Chemical Physics. 2010;**133**(11):114905

[13] Kovalchuk NM, Trybala A, Starov VM. Evaporation of sessile droplets. Current Opinion in Colloid and Interface Science. 2014;**19**(4):336-342

[14] Sefiane K. Patterns from drying drops. Advances in Colloid and Interface Science. 2014;**206**:372-381

[15] Wang JZ, Zheng ZH, Li HW, Huck WTS, Sirringhaus H. Dewetting of conducting polymer inkjet droplets on patterned surfaces. Nature Materials. 2004;**3**(3):171-176

[16] Dugas V, Broutin J, Souteyrand E. Droplet evaporation study applied to DNA chip manufacturing. Langmuir. 2005;**21**(20):9130-9136

[17] Trantum JR, Baglia ML, Eagleton ZE, Mernaugh RL, Haselton FR. Biosensor design based on Marangoni flow in an evaporating drop. Lab on a Chip. 2014;**14**(2):315-324

[18] Gulka CP, Swartz JD, Trantum JR, Davis KM, Peak CM, Denton AJ, et al. Coffee rings as low-resource diagnostics: Detection of the malaria biomarker *Plasmodium falciparum* histidine-rich protein-II using a surface-coupled ring of Ni(II)NTA gold-plated polystyrene particles. ACS Applied Materials & Interfaces. 2014;**6**(9):6257-6263

[19] Yakhno TA, Yakhno VG. Structural evolution of drying drops of biological fluids. Technical Physics. 2009;**54**(8):1219-1227

[20] Yakhno TA, Kazakov VV, Sanina OA, Sanin AG, Yakhno VG. Drops of biological fluids drying on a hard substrate: Variation of the morphology, weight, temperature, and mechanical properties. Technical Physics. 2010;**55**(7):929-935

[21] Rapis E. A change in the physical state of a nonequilibrium blood plasma protein film in patients with carcinoma. Technical Physics. 2002;**47**(4):510-512

[22] Bahmani L, Neysari M, Maleki M. The study of drying and pattern formation of whole human blood drops and the effect of thalassaemia and neonatal jaundice on the patterns. Colloids and Surfaces a-Physicochemical and Engineering Aspects. 2017;**513**:66-75

[23] Kokornaczyk MO, Dinelli G, Marotti I, Benedettelli S, Nani D, Betti L. Self-organized crystallization patterns from evaporating droplets of common wheat grain leakages as a potential tool for quality analysis. The Scientific World Journal. 2011;**11**:1712-1725

[24] Devlin NR, Loehr K, Harris MT. The separation of two different sized particles in an evaporating droplet. Aiche Journal. 2015;**61**(10):3547-3556

[25] Abdel-Mageed HM, Fouad SA, Teaima MH, Abdel-Aty AM, Fahmy AS, Shaker DS, et al. Optimization of nano spray drying parameters for production of α-amylase nanopowder for biotherapeutic applications using factorial design. Drying Technology. 2019:1-9. Available from: https://www.tandfonline.com/doi/full/10.1080/07373937.2019.1565576?scroll=top&needAccess=true

[26] Arpagaus C. A novel laboratory-scale spray dryer to produce nanoparticles. Drying Technology. 2012;**30**(10):1113-1121

[27] Trantum JR, Eagleton ZE, Patil CA, Tucker-Schwartz JM, Baglia ML, Skala MC, et al. Cross-sectional tracking of particle motion in evaporating drops: Flow fields and interfacial accumulation. Langmuir. 2013;**29**(21):6221-6231

[28] Manukyan S, Sauer HM, Roisman IV, Baldwin KA, Fairhurst DJ, Liang H, et al. Imaging internal flows in a drying sessile polymer dispersion drop using spectral radar optical coherence tomography (SR-OCT). Journal of Colloid and Interface Science. 2013;**395**:287-293

[29] Edwards AMJ, Atkinson PS, Cheung CS, Liang H, Fairhurst DJ, Ouali FF. Density-driven flows in evaporating binary liquid droplets. Physical Review Letters. 2018;**121**(18):184501

[30] Huang H, Huang YY, Lau W, Ou-Yang HD, Zhou C, El-Aasser MS. Integrating optical coherence tomography with gravimetric and video analysis (OCT-gravimetry-video method) for studying the drying process of polystyrene latex system. Scientific Reports. 2018;**8**:12962

[31] Lovell PA, El-Aasser MS. Emulsion Polymerization and Emulsion Polymers. 1997

[32] Deegan RD, Bakajin O, Dupont TF, Huber G, Nagel SR, Witten TA. Capillary flow as the cause

of ring stains from dried liquid drops. Nature. 1997;**389**:827-829

[33] Routh AF. Drying of thin colloidal films. Reports on Progress in Physics. 2013;**76**(4):046603

[34] Keddie J, Routh AF. Fundamentals of Latex Film Formation: Processes and Properties. Berlin: Springer Laboratory; 2010

[35] van der Kooij HM, Sprakel J. Watching paint dry; more exciting than it seems. Soft Matter. 2015;**11**(32):6353-6359

[36] Jovanovic R, Dube MA. Emulsion-based pressure-sensitive adhesives: A review. Journal of Macromolecular Science Polymer Reviews. 2004;**C44**(1):1-51

[37] Elgammal M, Schneider R, Gradzielski M. Preparation of latex nanoparticles using nanoemulsions obtained by the phase inversion composition (PIC) method and their application in textile printing. Colloids and Surfaces a-Physicochemical and Engineering Aspects. 2015;**470**:70-79

[38] Guan Y, Tawiah B, Zhang LP, Du CS, Fu SH. Preparation of UV-cured pigment/latex dispersion for textile inkjet printing. Colloids and Surfaces a-Physicochemical and Engineering Aspects. 2014;**462**:90-98

[39] Borase HP, Patil CD, Suryawanshi RK, Patil SV. Ficus carica latex-mediated synthesis of silver nanoparticles and its application as a chemophotoprotective agent. Applied Biochemistry and Biotechnology. 2013;**171**(3):676-688

[40] Najafi SMH, Tajvidi M, Bousfield DW. Production and mechanical characterization of free-standing pigmented paper coating layers with latex and starch as binder. Progress in Organic Coating. 2018;**123**:138-145

[41] Wu YM, Duan HD, Yu YQ, Zhang CG. Preparation and performance in paper coating of silicone-modified styrene-butyl acrylate copolymer latex. Journal of Applied Polymer Science. 2001;**79**(2):333-336

[42] Nakagami H, Keshikawa T, Matsumura M, Tsukamoto H. Application of aqueous suspensions and latex dispersions of water-insoluble polymers for tablet and granule coatings. Chemical & Pharmaceutical Bulletin. 1991;**39**(7):1837-1842

[43] Ladika M, Kalantar TH, Shao H, Dean SL, Harris JK, Sheskey PJ, et al. Polyampholyte acrylic latexes for tablet coating applications. Journal of Applied Polymer Science. 2014;**131**(7):12

[44] Brentin RP. Latex coating systems for carpet backing. Journal of Coated Fabrics. 1982;**12**(2):82-91

[45] Schulz M, Romermann H, Pohl K, Chindawong C, Johannsmann D. Latex films with In-plane composition gradients caused by lateral drying. Soft Materials. 2015;**13**(3):138-143

[46] Kolegov KS. Simulation of patterned glass film formation in the evaporating colloidal liquid under IR heating. Microgravity Science and Technology. 2018;**30**(1-2):113-120

[47] Georgiadis A, Muhamad FN, Utgenannt A, Keddie JL. Aesthetically textured, hard latex coatings by fast IR-assisted evaporative lithography. Progress in Organic Coating. 2013;**76**(12):1786-1791

[48] Routh AF, Russel WB. Horizontal drying fronts during solvent evaporation from latex films. Aiche Journal. 1998;**44**(9):2088-2098

[49] Divry V, Gromer A, Nassar M, Lambour C, Collin D, Holl Y. Drying mechanisms in plasticized latex films: Role of horizontal drying fronts. The

Journal of Physical Chemistry. B. 2016;**120**(27):6791-6802

[50] Routh AF, Zimmerman WB. Distribution of particles during solvent evaporation from films. Chemical Engineering Science. 2004;**59**(14):2961-2968

[51] Narita T, Hebraud P, Lequeux F. Effects of the rate of evaporation and film thickness on nonuniform drying of film-forming concentrated colloidal suspensions. European Physical Journal E. 2005;**17**(1):69-76

[52] Koenig AM, Weerakkody TG, KeddieJL,JohannsmannD.Heterogeneous drying of colloidal polymer films: Dependence on added salt. Langmuir. 2008;**24**(14):7580-7589

[53] Carter FT, Kowalczyk RM, Millichamp I, Chainey M, Keddie JL. Correlating particle deformation with water concentration profiles during latex film formation: Reasons that softer latex films take longer to dry. Langmuir. 2014;**30**(32):9672-9681

[54] Huang H. A novel dielectrophoresis potential spectroscopy for colloidal nanoparticles. Bethlehem: Lehigh University; Theses and Dissertations. 2018:4289

[55] Tirumkudulu MS, Russel WB. Cracking in drying latex films. Langmuir. 2005;**21**(11):4938-4948

[56] Tirumkudulu MS, Russel WB. Role of capillary stresses in film formation. Langmuir. 2004;**20**(7):2947-2961

[57] Birk-Braun N, Yunus K, Rees EJ, Schabel W, Routh AF. Generation of strength in a drying film: How fracture toughness depends on dispersion properties. Physical Review E. 2017;**95**(2):022610

[58] Francis LF, McCormick AV, Vaessen DM, Payne JA. Development and measurement of stress in polymer coatings. Journal of Materials Science. 2002;**37**(22):4717-4731

[59] Huang Y. Development of High-Speed Optical Coherence Tomography for Time-Lapse Non-Destructive Characterization of Samples. Bethlehem: Lehigh University; Theses and Dissertations. 2019:5564

[60] Routh AF, Russel WB. Deformation mechanisms during latex film formation: Experimental evidence. Industrial and Engineering Chemistry Research. 2001;**40**(20):4302-4308

[61] Lawman S, Liang HD. High precision dynamic multi-interface profilometry with optical coherence tomography. Applied Optics. 2011;**50**(32):6039-6048

[62] Saccon FAM, de Oliveira FMDR, Ribas MO, Zambianchi P, Muller M, Fabris JL. Kinetics of varnish long-term drying process monitored by a heterogeneous optical sensor system. Measurement Science and Technology. 2013;**24**(9):094013

[63] Yang B, Sharp JS, Smith MI. Shear banding in drying films of colloidal nanoparticles. ACS Nano. 2015;**9**(4):4077-4084

[64] Kiatkirakajorn P-C, Goehring L. Formation of shear bands in drying colloidal dispersions. Physical Review Letters. 2015;**115**(8):088302

[65] Huang Y, Badar M, Nitkowski A, Weinroth A, Tansu N, Zhou C. Wide-field high-speed space-division multiplexing optical coherence tomography using an integrated photonic device. Biomedical Optics Express. 2017;**8**(8):3856-3867

[66] Bouchaudy A, Salmon J-B. Drying-induced stresses before solidification in colloidal dispersions: In situ measurements. Soft Matter. 2019;**15**(13):2768-2781